



LAWRENCE
LIVERMORE
NATIONAL
LABORATORY

Lithium sputtering from lithium-coated plasma facing component in the NSTX divertor

F. Scotti, V. A. Soukhanovskii, J. -W. Ahn, R. E. Bell, S. P. Gerhardt, M. A. Jaworski, R. Kaita, H. W. Kugel, A. G. McLean, E. T. Meier, M. Podesta, A. L. Roquemore

May 22, 2014

21 International conference on plasma surface interactions on controlled fusion devices

Kanazawa, Japan

May 26, 2014 through May 30, 2014

Disclaimer

This document was prepared as an account of work sponsored by an agency of the United States government. Neither the United States government nor Lawrence Livermore National Security, LLC, nor any of their employees makes any warranty, expressed or implied, or assumes any legal liability or responsibility for the accuracy, completeness, or usefulness of any information, apparatus, product, or process disclosed, or represents that its use would not infringe privately owned rights. Reference herein to any specific commercial product, process, or service by trade name, trademark, manufacturer, or otherwise does not necessarily constitute or imply its endorsement, recommendation, or favoring by the United States government or Lawrence Livermore National Security, LLC. The views and opinions of authors expressed herein do not necessarily state or reflect those of the United States government or Lawrence Livermore National Security, LLC, and shall not be used for advertising or product endorsement purposes.

Lithium sputtering from lithium-coated plasma facing components in the NSTX divertor

F. Scotti^a, V.A. Soukhanovskii^a, J.-W. Ahn^c, R.E. Bell^b, S.P. Gerhardt^b, M.A. Jaworski^b, R. Kaita^b, H.W. Kugel^b, A.G. McLean^a, E.T. Meier^a, M. Podesta^b, A.L. Roquemore^b

^aLawrence Livermore National Laboratory, Livermore, CA, USA.

^bPrinceton Plasma Physics Laboratory, Princeton, 08540, NJ, USA.

^cOak Ridge National Laboratory, Oak Ridge, TN, USA.

Abstract

Lithium sputtering yields and gross impurity influxes from lithium-coated graphite and molybdenum plasma facing components (PFCs) in the National Spherical Torus Experiment (NSTX) divertor have been analyzed during H-mode NBI-heated discharges. Motivated by the beneficial effects of lithium conditioning on discharge performance and reproducibility, evaporative lithium coatings were the routine wall conditioning technique in NSTX. Neutral lithium sputtering yields from solid lithium coatings in NSTX were found to be consistent with values reported from test stand experiments from deuterium-saturated lithium (with sputtering yields $Y_{Li} \sim 0.03-0.07$). Temperature-enhanced lithium sputtering was observed on lithium-coated graphite and molybdenum as a result of PFC heating by both embedded heaters and incident plasma heat flux, leading to $Y_{Li} \sim 0.1-0.2$ for surface temperatures above the lithium melting point.

1. Introduction

In order to address the requirements for wall and divertor plasma facing components (PFCs), future fusion devices, such as ITER [1], will use several different materials as PFCs. Material erosion, migration and re-deposition, will lead to a mixed material environment, with properties which could differ from those of the virgin materials [2]. Understanding the synergies of different materials in terms of deuterium retention, sputtering, and potential for core contamination will be important for choosing PFCs in future machines.

The National Spherical Torus Experiment (NSTX) [3] employed mixed materials for the PFCs with lithium conditioning via evaporative coatings applied on graphite and molybdenum [4]. Accumulation of carbon impurities was routinely observed in the core of ELM-free lithium-conditioned discharges in NSTX [5]. Core lithium densities were less than 1% of the core carbon densities despite the large lithium depositions [6]. The different core impurity accumulation of carbon and lithium was only partially explained by the difference in their core radial transport [5] and motivated a deeper investigation of the sputtering and scrape-off layer (SOL) transport behavior of the two impurities in NSTX. This paper aims to characterize lithium sputtering yield and gross divertor influxes in NSTX.

2. Experimental setup and method

Several materials were employed in NSTX for the lower divertor PFCs starting from the 2010 experimental campaign. Two ATJ graphite tiles formed the inboard divertor ($R=28-57$ cm) while the outer divertor was composed of a graphite bullnose tile ($R=61-65$ cm), and the liquid lithium divertor (LLD, $R=65-84$ cm). The LLD consisted of four toroidal segments (each covering about 80° toroidally) of porous molybdenum ($\sim 170 \mu\text{m}$ thick with $0.1 \mu\text{m}$ characteristic porosity scale length) plasma sprayed on a stainless steel liner (0.25 mm thick) brazed to a copper plate (2.2 cm thick) with embedded heaters and thermocouples [7]. The four LLD plates were separated from each other by four instrumented graphite tiles.

Lithium coatings were applied on the NSTX lower divertor by two evaporators toroidally separated by 150° . Typical “doses” of 100-400 mg of lithium were evaporated before discharges. This “dose” corresponds to a “nominal”

lithium coating peak thickness of 20-80 nm or areal densities of $1-4 \times 10^{21}$ atoms/m², with a toroidal asymmetry in deposition up to a factor of 3 [4]. Effectively, chemical reactions with deuterium and vacuum impurities, erosion, evaporation and intercalation in graphite limited the lifetime of lithium coatings in NSTX [8]. The data presented in this paper are from the 2010 experimental campaign. Only lithiated conditions were available as a large lithium evaporation (16 g) was carried out before the beginning of plasma operation and no boronization was performed. By the end of the year, about 845 g of lithium were evaporated on the PFCs, which corresponds to areal densities up to 8×10^{24} atoms/m², neglecting erosion and intercalation. In this paper, lower single null, NBI-heated (2-6 MW), H-mode discharges with lithium conditioning are analyzed with attached outer strike point (OSP) conditions.

Impurity influxes from the PFCs are determined by means of divertor imaging cameras [9] filtered with narrow bandpass filters and interpreted via the ionizations per photon method (S/XB) [10] using coefficients from the ADAS database [11]. Two-dimensional cameras provide full coverage (radial and toroidal) of the lower divertor with 1-cm resolution [9]. The neutral lithium line at 670.9 nm (Li I) and singly ionized line at 548.5 nm (Li II) were used for the determination of lithium line integrated brightness. Incident ion fluxes are estimated by Langmuir probes. In discharges with OSP in the outer divertor, the high density Langmuir probe (HDLP) array [12] was used, which is located in one of the instrumented tiles and provides 4 single (swept at 1 kHz) and 5 triple (digitized at 250 kHz) probes at radii between 63 and 71 cm. Electron temperatures (T_e) and electron densities (n_e) from the HDLP array are used to determine S/XB coefficients. Uncertainties in T_e and J_{SAT} obtained from the fit of the classical I-V curve to the probe characteristic are propagated to determine the error in n_e and in the S/XB coefficients. S/XB coefficients are applied to line integrated brightness to infer impurity influxes, and impurity sputtering yields are then determined from the impurity influxes and the incident ion fluxes. For the comparison with tabulated values of sputtering yields, ion temperatures T_i , not measured on NSTX, are taken to be equal to T_e , leading to an incident ion energy of $5 \times T_e$ while the angle of incidence of the ions is assumed to be 45°.

3. Results and Discussion

The ability to heat the divertor PFCs with embedded heaters in NSTX enabled the possibility of testing the response of lithium influx and sputtering yield on molybdenum substrates as a function of the surface temperature (T_{surf}). In this section, two discharges are compared, both of which were carried out after a large lithium evaporation of 200 g (and a campaign-integrated lithium evaporation of 530 g), equivalent to a peak nominal coating thickness of $\sim 40 \mu\text{m}$. This thickness is larger than the LLD porosity and than the typical surface roughness of graphite in NSTX [13]. These discharges had similar plasma parameters ($P_{NBI} = 3 \text{ MW}$, $I_P = 900 \text{ kA}$, $I_P = 0.5 \text{ T}$, $\delta r_{sep} \sim -2 \text{ cm}$) and OSP in the lower outer divertor with peak divertor incident fluxes $\sim 1 \times 10^{23}$ ions/m²/s. Divertor T_e and n_e as measured by the Langmuir probes were in the range of 5–25 eV and $1 - 10 \times 10^{19} \text{ m}^{-3}$. In the first discharge (139598), three LLD plates were heated to $\sim 250^\circ\text{C}$ while one was left unheated due to the failure of the embedded heaters. In the second discharge (139769), all four LLD plates were left unheated and were below the lithium melting point ($T_m = 180.5^\circ\text{C}$). The first discharge was performed right after the large lithium evaporation while the second was carried out 130 discharges later (with an accumulated plasma exposure of $\sim 83 \text{ s}$ and an integrated ion fluence of $\sim 2 \times 10^{24}$ ions/m² at the 70.5 cm probe), without any pre-discharge (“fresh”) lithium evaporation. The integrated ion fluence was comparable to the lithium areal density from the 200 g evaporation, so the lithium coating is expected to be a deuterium-saturated lithium surface.

The higher T_{surf} on the heated LLD plates led to the local enhancement of lithium influxes with respect to unheated LLD plates and graphite. In Figure 1, contour plots of lower divertor Li I emission are plotted for the two discharges in consideration at $t = 0.5 \text{ s}$ as a function of the divertor radius R and toroidal angle ϕ . In Figure 1(a), higher lithium emission was observed on the three heated LLD segments ($R = 65-84 \text{ cm}$, $\phi = 10^\circ, 100^\circ, 280^\circ$), while emission on the graphite diagnostic tiles ($R = 65-84 \text{ cm}$, $\phi = 55^\circ, 145^\circ, 225^\circ$) was comparable to the emission on the unheated LLD plate ($R = 65-84 \text{ cm}$, $\phi = 190^\circ$). In contrast, in the discharge where all the LLD plates were unheated (Figure 1(b)) no clear difference was observed between the various LLD segments. The relative enhancement in lithium influxes can be seen more effectively from the ratio of the brightness at a given radial location in the two discharges, plotted in Figure 1(c) as a function of ϕ . This normalization is also useful to correct for the residual asymmetry in the toroidal profile of lithium brightness which cannot be accounted for by the 2D calibration. While no difference was observed on graphite and on the LLD plate which was unheated in both discharges, an enhancement of a factor up to 1.5-2 was seen over the heated plates when their temperature is above the lithium melting point. In the same plot, the bulk

temperatures of the copper plates are plotted for the two discharges as measured by the embedded thermocouples. This enhancement is qualitatively consistent with the temperature-enhanced (“thermal”) sputtering observed on test stands (PISCES [14, 15] and IIAX [16]), which was attributed to the dependence of the lithium surface binding energy on T_{surf} . From the contour plots in Figure 1, no clear difference in neutral lithium emission can be observed between unheated molybdenum and graphite substrates. This is further evident from the radial profiles on graphite and unheated LLD plotted in Figure 1(d)-(e) (blue and green curves). While a reduction in lithium sputtering was measured on lithiated graphite in IIAX [17] and was attributed to the formation of ionic bonds between carbon and lithium, the NSTX result can be understood as due to the macroscopically thick lithium coatings, which reduce the role of the substrate in determining the surface sputtering. It must be noted here that while plasma parameters are assumed to be toroidally uniform, any local increase in n_e due to the higher lithium influxes on the heated plates would further augment this enhancement due to the dependence of the Li I S/XB coefficient on n_e and its insensitivity to T_e . The measured local lithium influxes are $\sim 1 \times 10^{21}$ - 1×10^{22} atoms/m²/s, several orders of magnitude larger than the evaporative fluxes expected at $T_{surf} \sim 200$ - 300° (up to 1×10^{19} atoms/m²/s). Measured lithium influxes are therefore due to lithium physical and “thermal” sputtering and can be used for the determination of the effective sputtering yield Y_{Li} .

Sputtering yields determined on solid and liquid lithium coatings in NSTX were consistent with expectations from physical and “thermal” sputtering from deuterium saturated lithium. In Figure 2(a)-(b), temporal waveforms of lithium influxes (a) at one of the triple probe locations ($R = 71$ cm) and the inferred neutral lithium sputtering yields are plotted as a function of time as measured on graphite (diagnostic tile - black) and molybdenum (heated LLD plate - red, and unheated LLD plate - blue). While the local influxes at the probe location vary by as much as an order of magnitude during the discharge due to the drift of the OSP over time, the inferred local sputtering yield was constant as a result of the weak dependence of Y_{Li} on the incident energy above the sputtering threshold and the relatively unchanged T_{surf} . The measured values of $Y_{Li} \sim 3$ - 7% are consistent with estimates from *bca* codes (SRIM-TRIM [18]) and values reported from test stand experiments on deuterium-saturated lithium surfaces. Presumably due to thick lithium coatings, the difference between lithium sputtering yields on the graphite tile and on the unheated molybdenum plate is marginal (black and blue trace) throughout the entire discharge. In contrast, an enhancement of up to a factor of 2 was observed as a result of the heating of the PFCs to 250°C (red vs. blue trace). This is also seen in the radial profiles of lithium sputtering yields as a function of $R - R_{OSP}$ shown in Figure 2(c), where yields calculated at two triple probe locations ($R = 63, 71$ cm) have been included during a 100 ms sweep of the OSP location. It can also be noticed that the sputtering yields calculated on the bullnose graphite tile ($R = 63$ cm) do not systematically vary at the three different toroidal locations, in contrast to the measurements at $R = 71$ cm.

The response of the lithium sputtering yield to changes in T_{surf} (as a result of heating due to the local plasma heat flux), has also been studied on graphite substrates, showing agreement with expectations from deuterium-saturated liquid lithium. In Figure 3, lithium sputtering yield as measured in discharge 139769 at several probe locations ($R=63,64,67$ cm) in the vicinity of the strike point is plotted as a function of the T_{surf} measured by the two-color IR camera [19]. In this plot, error bars include also the variability of the lithium influxes and T_{surf} over the toroidal angle (4°) used for the averaging of the IR and spectroscopic measurements. To minimize the effect of leading edges on the lithium sputtering estimates (evident from the contour plots in Figure 1(a)-(b) and from IR thermography), toroidal averaging was performed on the central part of the graphite tile with the largest toroidal extent. Measurements of the lithium sputtering yield over a range of T_{surf} between 50°C and 500°C were obtained, with Y_{Li} up to 0.25. In Figure 3, neutral lithium sputtering yield from a VFTRIM-3D semi-empirical model by J.P. Allain based on IIAX results [20] for deuterium incident at 45° and 50 eV on deuterium-saturated lithium is also plotted showing reasonable agreement with the NSTX data.

While the effective lithium sputtering yield measured on thick lithium coatings in NSTX is consistent with expectations from physical and “thermal” sputtering due to deuterium incident on deuterium-saturated lithium, it must be noted that the lithium surface in NSTX can be contaminated with carbon and oxygen [21]. Furthermore, the effect of lithium sputtering due to impurities (self-sputtering and carbon) was not included. Due to the relatively similar Y_{Li} due to incident deuterium (Y_{Li-D}), carbon (Y_{Li-C}) and lithium (Y_{Li-Li}) ions at typical NSTX divertor incident energies (~ 50 - 100 eV), the inclusion of sputtering due to impurities is not expected to significantly affect the results. While the carbon contribution is negligible, the inclusion of lithium self-sputtering could lead to a deviation of Y_{Li-D} from the measured effective yield, Y_{Li} . However, for the highest Y_{Li} case in this work (~ 0.2), and assuming 100% re-deposition, the measured effective Y_{Li} would overestimate Y_{Li-D} by only 15%, thus not affecting the conclusions.

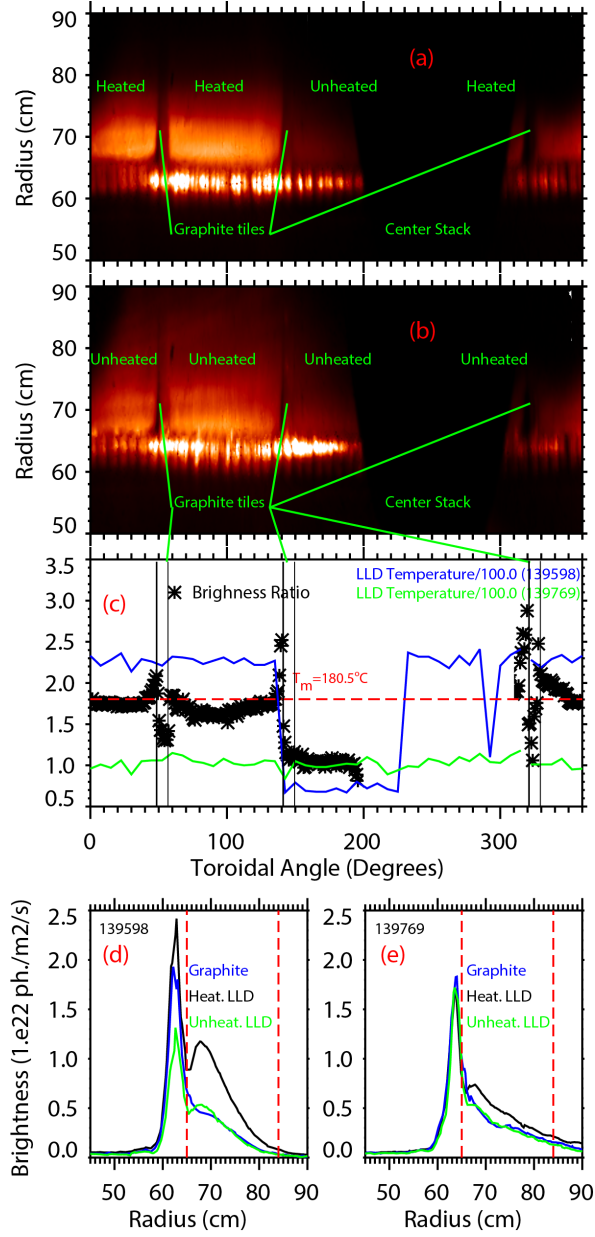


Figure 1: Li I emission in discharge 139598 (a) and 139769 (b), ratio of the line integrated brightness as a function of ϕ at $R = 70$ cm (c), and radial profiles of Li I brightness in discharge 139598 (d) and 139769 (e).

Further complicating factors in the interpretation of these results are the possibly different sputtering behavior of re-deposited lithium layers with respect to freshly evaporated coatings (e.g., as observed for beryllium in PISCES [2]) and the possible contribution of lithium droplet ejection to the measured lithium influxes.

Despite the large gross lithium influxes, re-deposition effects are expected to play an important role in regulating both the lifetime of lithium coatings and the core contamination of lithium ions in NSTX. Even with more typical lithium “doses” (~ few 100s mg), sputtering yields comparable to those presented in this section have been measured, without indications of decreasing lithium influxes over the course of 1 s NSTX discharges. This is suggestive of the importance of re-deposition effects but the relative role of accumulated vs “fresh” lithium coatings on the lithium influxes in NSTX still needs to be better characterized. A large prompt re-deposition fraction (resulting from the

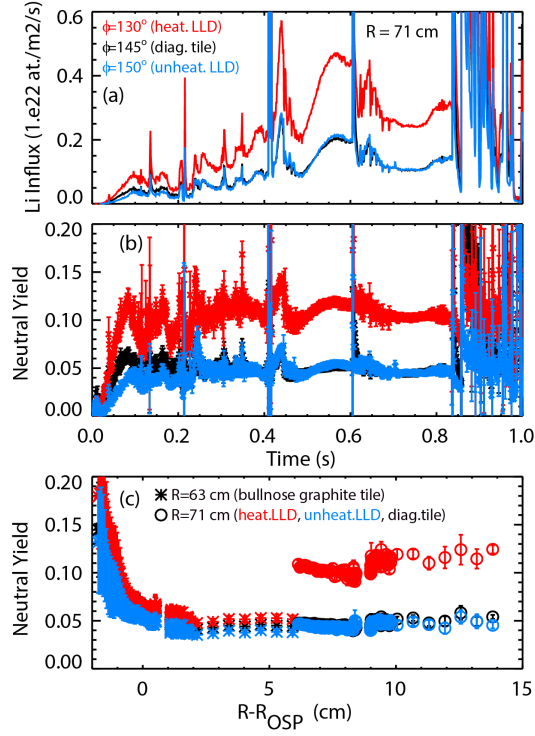


Figure 2: Neutral lithium influxes and sputtering yield from the probe at $R=71$ cm as a function of time (a, b) at three different toroidal locations: graphite tile (black), heated LLD (red) and unheated LLD (blue). Neutral lithium sputtering yields at the same toroidal locations as a function of $R - R_{OSP}$ from the probe at $R=71$ cm (circles) and at $R=63$ cm (stars).

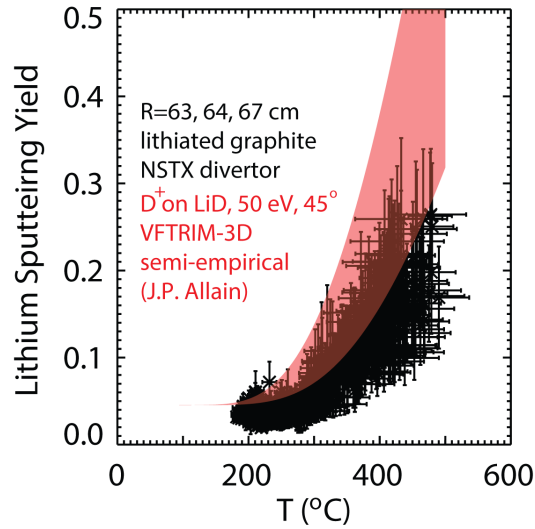


Figure 3: Neutral lithium sputtering yield as a function of surface temperature from lithium coated graphite tiles.

ionization mean free path being much shorter than the ion gyro-radius) was predicted by kinetic simulations with WBC-REDEP [20] and is consistent with the measurements of singly ionized lithium influxes, which are typically ~ 1 or 2 orders of magnitude lower than the neutral lithium influxes at the OSP. Integrating the OSP neutral lithium influxes, gross lithium influxes in NSTX H-modes are estimated at $\sim 1 - 5 \times 10^{21}$ atoms/s. Comparing the gross

influxes with the lithium core particle inventories ($\sim 1 - 3 \times 10^{17}$ ions) as measured by charge exchange recombination spectroscopy [6], very low penetration factors are determined ($\sim 1 \times 10^{-4} - 1 \times 10^{-3}$). This is much less than what inferred for carbon ($\sim 1 \times 10^{-1}$) and can be associated with the very good divertor retention of lithium as a result of both prompt re-deposition and the effect of classical parallel SOL forces, as evident from UEDGE simulations.

4. Conclusions

Lithium sputtering yields and gross impurity influxes from lithium-coated divertor PFCs have been analyzed in H-mode NBI-heated discharges in NSTX. Neutral lithium sputtering yields from lithium coatings were found to be consistent with values reported from test stand experiments from solid and liquid deuterium-saturated lithium, with Y_{Li} up to ~ 0.2 . The very low lithium core contamination observed on NSTX, combined with the low atomic number, offers a great opportunity for the use of lithium as a PFC in current and future fusion devices. Large influxes of lithium at the target may be exploited to control divertor heat flux (thanks to the increased density and radiation), while allowing minimal core contamination. Studying the behavior of lithium coatings in ITER-relevant divertor heat and particle fluxes in NSTX-U will clarify the potential for the application of solid/liquid lithium PFCs in future fusion reactors.

5. Acknowledgments

This work was supported by U.S. DOE Contracts: DE-AC02-09CH11466, DE-AC52-07NA27344, DE-AC05-00OR22725. The authors would like to acknowledge Prof. J.P. Allain for the reference sputtering data.

References

- [1] ITER Physics Expert Group on divertor, Nucl. Fusion 39 (1999) 2391.
- [2] R. Doerner, et al., Nucl. Fusion 52 (2012) 103003.
- [3] M. Ono, et al., Nucl. Fusion 40 (2000) 557.
- [4] H. Kugel, et al., Phys. Plasmas 15 (2008) 056118.
- [5] F. Scotti, et al., Nucl. Fusion 53 (2013) 083001.
- [6] M. Podesta', et al., Nucl. Fusion 52 (2012) 033008.
- [7] H. Kugel, et al., Fusion Eng. Des. 84 (2009) 1125–1129.
- [8] W. Wampler, et al., J. Nucl. Mat. 390-391 (2009) 1009–1012.
- [9] F. Scotti, et al., Rev. Sci. Instrum. 83 (2012) 10E532.
- [10] K. Behringer, et al., Plasma Phys. Control. Fusion 31 (1989) 2059.
- [11] H.P. Summers, The ADAS User Manual, <http://www.adas.ac.uk>, (2004).
- [12] J. Kallman, et al., Rev. Sci. Instrum. 81 (2010) 10E117.
- [13] C. Taylor, et al., New Journal of Physics Submitted.
- [14] R. Doerner, et al., J. Nucl. Mat. 290-293 (2001) 166–172.
- [15] R. Doerner, et al., J. Nucl. Mat. 313-316 (2003) 383–387.
- [16] J. Allain, et al., Phys. Rev. B 76 (2007) 205434.
- [17] M. Racic, et al., J. Nucl. Mat. 390-391 (2009) 1043–1047.
- [18] <http://www.srim.org/>.
- [19] A. Mclean, et al., Rev. Sci. Instrum. 83 (2012) 053706.
- [20] J. Allain, et al., Nucl. Fusion 51 (2011) 023002.
- [21] C. Skinner, et al., J. Nucl. Mat. 438 (2013) S647-S650.